



Novel ultra-wideband fluorescence material: Defect state control based on nickel-doped semiconductor QDs embedded in inorganic glasses

Z. Wang, F. Huang, M. Cai, X. Zhang, D. Deng, S. Xu

► To cite this version:

Z. Wang, F. Huang, M. Cai, X. Zhang, D. Deng, et al.. Novel ultra-wideband fluorescence material: Defect state control based on nickel-doped semiconductor QDs embedded in inorganic glasses. *Journal of Materiomics*, 2023, 9 (2), pp.338-344. <10.1016/j.jmat.2022.10.001>. <hal-04066374>

HAL Id: hal-04066374

<https://hal.science/hal-04066374v1>

Submitted on 30 May 2023

HAL is a multi-disciplinary open access archive for the deposit and dissemination of scientific research documents, whether they are published or not. The documents may come from teaching and research institutions in France or abroad, or from public or private research centers.

L'archive ouverte pluridisciplinaire **HAL**, est destinée au dépôt et à la diffusion de documents scientifiques de niveau recherche, publiés ou non, émanant des établissements d'enseignement et de recherche français ou étrangers, des laboratoires publics ou privés.

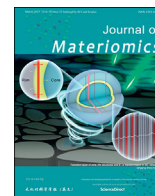


HAL Authorization



Contents lists available at ScienceDirect

Journal of Materiomics

journal homepage: www.journals.elsevier.com/journal-of-materiomics/

Novel ultra-wideband fluorescence material: Defect state control based on nickel-doped semiconductor QDs embedded in inorganic glasses

Zheng Wang^{a, b}, Feifei Huang^{a, *}, Muzhi Cai^a, Xianghua Zhang^b, Degang Deng^a,
Shiqing Xu^{a, **}

^a Key Laboratory of Rare Earth Optoelectronic Materials and Devices of Zhejiang Province, Institute of Optoelectronic Materials and Devices, China Jiliang University, Hangzhou, 310018, China

^b Laboratory of Glasses and Ceramics, Institut des Sciences Chimiques de Rennes, UMR CNRS 6226, University of Rennes 1, Rennes, 35042, France

ARTICLE INFO

Article history:

Received 7 September 2022

Received in revised form

9 October 2022

Accepted 12 October 2022

Available online 26 October 2022

Keywords:

ZnS quantum dots glass

Nickel-doping

Defect states

Broad-band emission

ABSTRACT

In recent years, the development of an environmentally friendly quantum dots (QDs) embedded luminous solid by a simple method has attracted considerable attention. In this study, semiconductor ZnS QDs were successfully prepared in an inorganic matrix of amorphous glass, which yielded beneficial broad-band emission in the long-wavelength region of the visible range. The strong red emission belonged to the defect state energy level of the ZnS QDs, which could be enhanced by incorporation of nickel ions into the fixed matrix to regulate the defects state. The novel material had a small self-absorption, wide excitation and emission ranges, and thus potential applications in light-conversion devices, luminescent solar concentrators, and solar cell cover glasses.

© 2022 The Authors. Published by Elsevier B.V. on behalf of The Chinese Ceramic Society. This is an open access article under the CC BY-NC-ND license (<http://creativecommons.org/licenses/by-nc-nd/4.0/>).

1. Introduction

Owing to their incredible size effect, semiconductor QDs exhibit excellent optoelectronic properties in the application of displays, light-emitting diodes, lasers, and luminescent solar concentrators, and have become one of the most actively investigated materials in recent decades [1–8]. Various high-quality semiconductor QDs such as IIB-VIA (ZnS, ZnSe, ZnTe, CdS, CdSe, CdTe, etc.), IVB-VIA (PbS, PbSe, PbTe, etc.), and halide perovskite (CsPbBr₃, etc.) QDs have been successfully synthesized [9–13]. Continuous theoretical and experimental studies led to unprecedented developments in semiconductor QD materials, from synthesis to performance enhancement [4,7,14–17]. However, most colloidal QDs synthesized by the wet chemical method are unstable and sensitive to the atmospheric environment [5,12,18]. Inorganic amorphous glasses can be easily processed and have been proved to possess good

optical properties [19,20]. Furthermore, the high density and uniform composition can protect the QDs from the surrounding environment [12]. The aggregation or dissolution of QD particles can be prevented in glass hosts. In addition, the size and distribution of the embedded QDs can be effectively controlled [21]. Compared to inorganic amorphous glass, host materials such as polymers and sol-gel films are chemically and mechanically unstable, and their applications in optoelectronic devices are subject to certain restrictions [12,18]. Therefore, QD glasses can fully utilize the advantages of QDs and inorganic amorphous glass, which are well promising optical materials.

As a specific type of glass ceramics that do not participate in the crystallization of the network formers [22], the QD glasses embedded with semiconductor QDs of group II-VI and IV-VI elements and perovskite QDs prepared by the co-melting heat treatment method have attracted considerable interest [12,18,21,23]. The luminescence properties of QDs embedded in inorganic glass, including the spectral range and luminous intensity, are generally similar to those of the corresponding colloidal QDs [12,24]. However, almost all main components of the QD glasses with high performances that are currently developed contain heavy metal elements such as Cd or Pb, which are harmful to the human body and are not environment-friendly [12].

* Corresponding author.

** Corresponding author.

E-mail addresses: huangfeifei@cjl.u.edu.cn (F. Huang), shiqingxu@cjl.u.edu.cn (S. Xu).

Peer review under responsibility of The Chinese Ceramic Society.

Although Cd chalcogenide, Pb chalcogenide, and Pb-halide perovskite nanocrystals embedded glasses have been considered as a promising materials in recent years, they are still not suitable for large-scale applications because of the toxicity of Pb and Cd elements [18]. Therefore, non-toxicity or low-toxicity environmentally friendly QD glasses with simple preparations and stable performances are required. As a typical II–VI group semiconductor material, ZnS exhibits a wide direct optical bandgap with a large exciton binding energy in the bulk at room temperature and is used as the shell structure of core-shell QDs [4,25]. However, the radiative transition of bare ZnS is limited within the blue-light region of the electromagnetic spectrum, which restricts its further application [12]. Doping with activated ions (such as rare earth and transition metal ions) can effectively control the photoelectromagnetic properties of QDs and broaden the application range of QDs, which has been extensively investigated for the synthesis and optical applications of colloidal QDs [26–31]. Transition metal elements (such as Cr, Mn, Co, Ni, Cu) exhibit abundant spectral characteristics in the visible to infrared range [32–38], and their ionic radii are similar to that of zinc. It is significant to investigate co-doping of these optical ions with low-toxicity ZnS in the glass to control and obtain QD glasses with specific optical properties. However, the number of valence states of elements such as Cr, Mn, Co, and Cu is more complex and they are difficult to control [39], while nickel ions have relatively stable valence states and radii closer to those of zinc ions. Thus, they are ideal dopants to adjust the optical properties of the ZnS QD glass. However, ZnS contains S^{2-} which is easily oxidized during the high-temperature melting of the glass, which hinders the precipitation ZnS in the glass [40]. Therefore, studies on nickel ions introduced into the ZnS QD glass as dopants to adjust their optical properties are temporary vacancy and need to be investigated.

In this study, we prepared and analyzed an environment-friendly ZnS QD-embedded glass. The proper optical basicity of the glass host components ensures the precipitation conditions of the ZnS QDs from the amorphous environment, which can be prepared by the convenient co-melting method. Co-doping with nickel ions promotes the precipitation and growth of ZnS QDs and further leads to an increased and more stable defect-state energy level, thereby providing an enhanced and stable broadband red fluorescence emission.

2. Experimental

All the raw materials are mixed uniformly in an agate mortar and then placed in a corundum crucible, and melted in a resistance furnace at 1400 °C for 40 min. The obtained melt is quenched and pressed on a preheating plate and then annealed or heat-treated in an annealing furnace to obtain the initial samples. For the structure and properties related to testing, the initial sample required other appropriate cutting, grinding, or polishing processes.

X-ray diffraction (XRD) measurements were performed on the samples using a D/MAX2550pc diffractometer (Rigaku International Co., Japan) and $Cu K_{\alpha 1}$ as the incident radiation source to obtain information on the structural analysis. To obtain the microstructure information of the samples, the scanning transmission electron microscopy (STEM) was measured using Tecnai G2 F20 (FEI, USA) high-resolution transmission electron microscope (HRTEM), operating at 200 kV with the current on specimen ~50 pA. The optical absorption spectra were recorded on a Hitachi U-4100 ultraviolet–visible–near-infrared (UV–VIS–NIR) spectrophotometer. The photoluminescence (PL) emission spectra, PL excitation spectra, PL quantum yields (PLQYs), and luminescence lifetime measurements were performed on an FLSP920 spectrometer (Edinburgh Instrument Ltd., Livingston, UK) equipped with a Xe-lamp and μs flash lamp as excitation sources.

3. Results and discussion

This glass system containing three typical glass network formations, SiO_2 , GeO_2 , and B_2O_3 , was designed. Notably, S^{2-} ions are easily oxidized at high temperatures. A certain optical basicity is necessary for the glass system to reduce the possibility of oxidation [40]. Moreover, the matrix composition contains glass network modification bodies such as Al_2O_3 , Na_2O , ZnF_2 and NaF. Fluoride components such as NaF are used to reduce the melting point and phonon energy of the system. The excess Zn^{2+} ions provided by ZnF_2 also have the effect of locking S^{2-} ions in the system [40]. Therefore, the specifically designed glass component of the precursor glass (PG) is $20SiO_2-30GeO_2-10B_2O_3-15Al_2O_3-10ZnF_2-10Na_2O-5NaF$ (1%, in mole). The optical basicity of the system can be determined based on the Duffy's empirical formula [41,42].

$$\begin{aligned} A = & x_{SiO_2} \cdot A(SiO_2) + x_{GeO_2} \cdot A(GeO_2) + x_{B_2O_3} \cdot A(B_2O_3) \\ & + x_{Al_2O_3} \cdot A(Al_2O_3) + x_{ZnF_2} \cdot A(ZnF_2) + x_{Na_2O} \cdot A(Na_2O) + x_{NaF} \cdot A(NaF) \end{aligned} \quad (1)$$

Where x_{SiO_2} , x_{GeO_2} , $x_{B_2O_3}$, $x_{Al_2O_3}$, x_{ZnF_2} , x_{Na_2O} , x_{NaF} and $A(SiO_2)$, $A(GeO_2)$, $A(B_2O_3)$, $A(Al_2O_3)$, $A(ZnF_2)$, $A(Na_2O)$, $A(NaF)$ are the molar fractions and optical basicity values of the glass components, respectively. Correspondingly, the optical basicity of the present glass was calculated to be 0.568 based on the optical basicity values of SiO_2 (0.476), GeO_2 (0.60), B_2O_3 (0.42), Al_2O_3 (0.606), Na_2O (1.15), ZnF_2 (0.475), and NaF (0.55) [41,42], which is below the reported critical value of 0.585 and is beneficial for the reduction in the oxidation of S^{2-} ions [40,41]. As the most important QD components and trace dopants in the system, ZnS and NiO are introduced in the raw material mixing process in the form of powders. The corresponding samples can be obtained by a convenient co-melting method from the designed glass components and dopants. The specific experimental process is described in the Supporting Information.

The amount of ZnS introduced in the system was determined by comprehensively considering the optical quality of amorphous glass and possible effects on luminescence properties. Fig. S1 shows the photoluminescence curves of the glass under short-wave ultraviolet excitation under different ZnS doping levels. The characteristic emission peak at 427 nm corresponding to the ZnS QDs of the sample increased with the amount of doped ZnS [24]. We believe that, with the above ZnS content (2%, 4% and 6%, in mass), ZnS QDs can already be precipitated in the preformed glass. However, considering the stability of the glass system and limited reduction environment (owing to the optical basicity of the system), the content of ZnS cannot be increased indefinitely, which will cause increased bubbles and devitrification of phase separation in the glass. When the concentration reached 6%, more obvious bubbles were produced in the prepared glass, as shown in Fig. S2a. Therefore, to maintain the excellent optical performance of the system, the content of 4% was considered to be more appropriate content. This content was also used as the ZnS content benchmark in the subsequent experimental process.

To investigate the structures of the samples and verify the existence of ZnS QDs in the glass, we performed X-ray diffraction (XRD) on all samples, as shown in Fig. S3. There is no obvious difference among the XRD curves of the PG, the nickel single-doped sample (denoted as NG), and heat-treated (at 600 °C for 10 h) hosts (denoted as PGA and NGA, respectively). They exhibit two broad humps, which indicates the good amorphous structure of the primary synthetic host [43]. This indicates that the incorporation of a small amount of nickel ions and heat-treatment had a very weak effect on the amorphous structure of these glass systems. However,

there are still no obvious diffraction peaks in the XRD curves of the 4%–ZnS doped sample (denoted as ZG), ZG after heat treatment at 600 °C for approximately 10 h (denoted as ZGA), and samples before (denoted as NZ) and after (denoted as NZA) heat-treatment of the co-doped ZnS and nickel ions. Nonetheless, it should not be ignored that the peak shape of the sample doped with ZnS has a certain broadening and that the peak position has a certain degree of shift compared to the sample without ZnS doping, particularly the co-doped sample after heat treatment (NZA). Thus, the structures of these samples changed compared to those of the samples without ZnS doping. Notably, no obvious characteristic diffraction peaks of ZnS were detected, presumably due to the small crystalline size and good dispersion of ZnS, which needs to be confirmed by subsequent TEM images. To analyze the microstructures, we conducted HRTEM on the samples. The TEM image of the NZA sample shows numerous nanocrystalline phases uniformly distributed in the amorphous glass, with a size of approximately 6 nm, as shown in Fig. 1b. Moreover, the HRTEM image shows clear crystal lattice fringes. The spacing between the two crystal planes was approximately 0.291 nm, as shown in Fig. 1c, which corresponds to the (0 1 2) crystal plane of ZnS [44,45]. In addition, the TEM image of the NZ sample shows numerous uniformly distributed small black spots in the amorphous glass phase, with a size of approximately 2 nm, as shown in Fig. 1a. Thus, at least in the hot press molding or during the annealing process of the sample preparation, the ZnS crystal phase was separated in the system. However, there is no direct and effective evidence of the precipitation of ZnS QDs in the TEM images of the ZG and ZGA samples. A possible reason is that, only ZnS is used as a dopant in the glass system (ZG), ZnS will precipitate in the form of amorphous micro-clusters and crystal nuclei or few QDs through phase separation during the cooling of the melt. Further long heat treatment process (ZGA) strengthens this phase. When nickel ions are co-incorporated into the system, they further participate as nucleating agents to induce this separation process, leading to more and larger ZnS QDs.

Fig. 2a and 2b shows ultraviolet–visible–near-infrared (UV–VIS–NIR) absorption spectra of different samples before and after heat treatment, respectively, where the corresponding absorption bands are appropriately labeled. In the absorption spectra of the PG and PGA samples, no other obvious absorption peaks were observed, except for the UV cut-off absorption. The two broad bands in the absorption spectra of the Ni²⁺ ion single doped samples (NG, NGA) at 428 and 815 nm correspond to Ni²⁺: ³E'(F) → ³E''(F) and Ni²⁺: ³E'(F) → ³A₂(F) of the tetrahedral in amorphous matrix [46], respectively. Notably, the UV absorption cut-off wavelength of the ZnS-doped samples (ZG, ZGA) has a certain red-shift relative to the undoped samples, and the blue shift

is more obvious with the heat treatment or the increased doping amount as shown in Fig. S4a. Since the electrophilic potential of S²⁻ ions is smaller than that of both O²⁻ and F⁻ ions, the addition of ZnS will inevitably lead to a red shift of the UV absorption cut-off edge. Meanwhile, considering the results of the XRD and TEM tests, this phenomenon can also be explained that the few ZnS QDs and other forms (amorphous clusters) of ZnS precipitated in the ZG, and ZGA samples. In NZ and NZA, the addition of nickel ions has a certain effect on reducing the surface energy barrier of ZnS nucleation growth, which facilitated the precipitation of ZnS QDs in the samples and smoothly growth. Therefore, in addition to the absorption spectra of the co-doped samples (NZ, NZA) with the typical absorption bands of the nickel ions (compared to the ZG and ZGA samples single doped with ZnS), the UV cut-off wavelength has different degrees of red-shift (compared to ZG, ZGA, NG and NGA samples single doped with ZnS or nickel ions, respectively), as shown in Figs. S4b and S4c. The reason for this phenomenon can be explained by the absorption of the band gap and defect energy levels of the precipitated ZnS QDs. Moreover, considering the experience on glass-ceramics, this phenomenon could also be partly attributed to the Rayleigh scattering caused by the ZnS crystal phase with a certain size in the sample [22], which can also explain the more obvious red-shift of the heat-treated co-doped sample.

To analyze the optical properties of the samples, photoluminescence spectra of all samples were measured at an excitation wavelength of 365 nm, as shown in Fig. 3a and 3b. The undoped and single-doped nickel samples before and after heat treatment (PG, PGA, NG and NGA samples, respectively) did not exhibit obvious emission in the test band (380–850 nm), which is consistent with the photographs of the samples under UV light, as shown in Fig. S2c. Both ZG and ZGA have an obvious luminescence at 427 nm, which can be attributed to the emission of ZnS QD defect states. Moreover, as the ZGA samples precipitated more ZnS QDs after the heat treatment process, their emission at this wavelength was improved to a certain extent. Furthermore, in addition to the fluorescence around 427 nm, ZGA exhibited a very weak fluorescence emission near the center of 640 nm. Owing to the dual-band fluorescence emission effect, the samples exhibit a weak blue-violet luminous color under a commercial 365 nm UV lamp radiation, as shown in Fig. S2c. The energy corresponding to these peaks is smaller than the bandgap of ZnS. Therefore, these two emissions can be attributed to the transition between discrete energy levels in the bandgap of ZnS QDs. The emission at 427 nm is generally attributed to the recombination of electrons trapped by S vacancies with holes in the valence band in the ZnS QDs [47–49]. And the long-wave emission at approximately 640 nm is generally

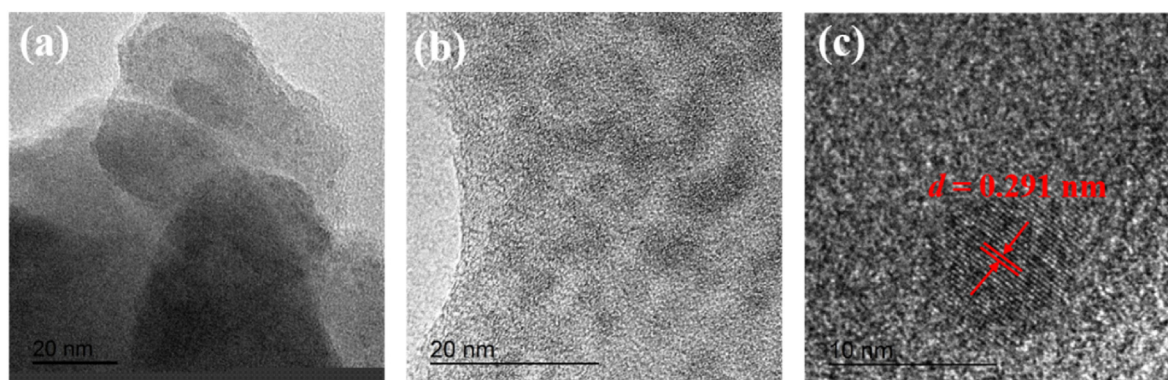


Fig. 1. Transmission electron microscopy (TEM) images of the NZ (a) and NZA (b) samples and high-resolution (HR)TEM image of NZA sample (c).

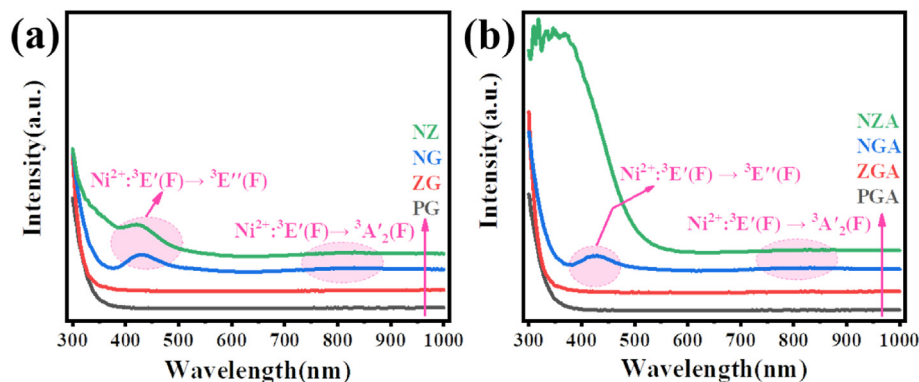


Fig. 2. Absorption spectra of glass samples (a) and samples after heat treatment (b) with different doping conditions.

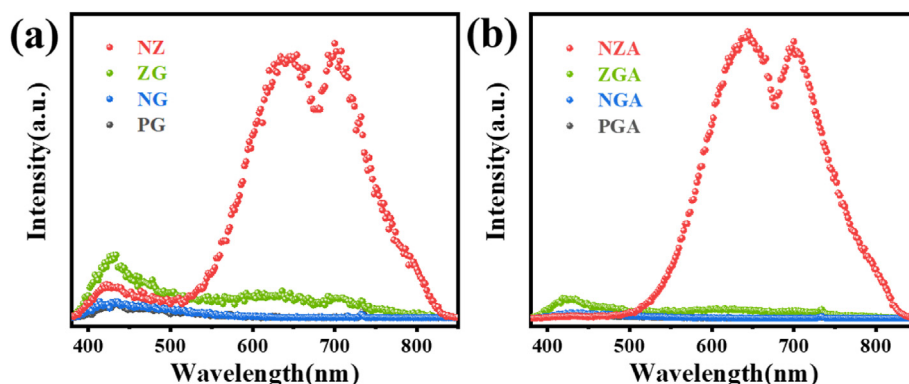


Fig. 3. Photoluminescence spectra of samples with different doping conditions before (a) and after (b) heat treatment under 365 nm pumping.

attributed to recombination of electrons trapped by S vacancies with holes trapped by Zn vacancies [47]. Based on the above information, a simple schematic of the optical recombination mechanism is presented in Fig. 5d, which is consistent with the photoluminescence principle and phenomenon of colloidal QDs. The luminescence phenomena above the ZG and ZGA samples are consistent with that of ZnS colloidal QDs, which is also a good proof of the existence of ZnS QDs in the above samples [33]. However, in this case, the amount of precipitated ZnS QDs may be limited, which is not ideal in terms of structural testing or spectral intensity.

When nickel ions were also introduced into the system, the NZ and NZA samples exhibited strong wide-band emissions with different intensities in the range of 500–830 nm. The luminescence of NZA was significantly enhanced after the heat-treatment. This can be explained as nickel ions (1) may act as impurity ions to precipitate more ZnS and (2) enter the ZnS QDs and provide added and more stable defect states. The main manifestation is the more easily detectable TEM morphology of NZ and NZA and stronger and wider long-wavelength emission of the visible light range. Owing to this emission, NZ and NZA exhibited a deep red luminous color under the commercial 365 nm UV lamp radiation, as shown in Fig. S2c. To the best of our knowledge, regardless of colloidal QDs or QD glasses, there is no report that nickel ion-doped ZnS QD materials exhibit a broad-band deep-red luminescence [12,24,26]. The studies on the luminescence of nickel ions-doped glass materials have also focused on its use in tunable near-infrared broadband luminescence [32,50,51], except that S. Buddhudu *et al.* obtained a narrow linewidth emission (full width at half maximum FWHM~10 nm) of nickel ions at 670 nm on borate glass [52,53]. The fluorescence decay times of the above luminous peaks show that

both weak emission in the short-wave region and strong emission in the long-wave region are within nanoseconds (Detailed data of the life decay fit are presented in Table S2 and Table S3 in the Supporting Information.), as shown in Figs. S5 and S6. This indicates that the fluorescence of the series of samples should not be derived from ion emission. Moreover, the photoluminescence spectra of

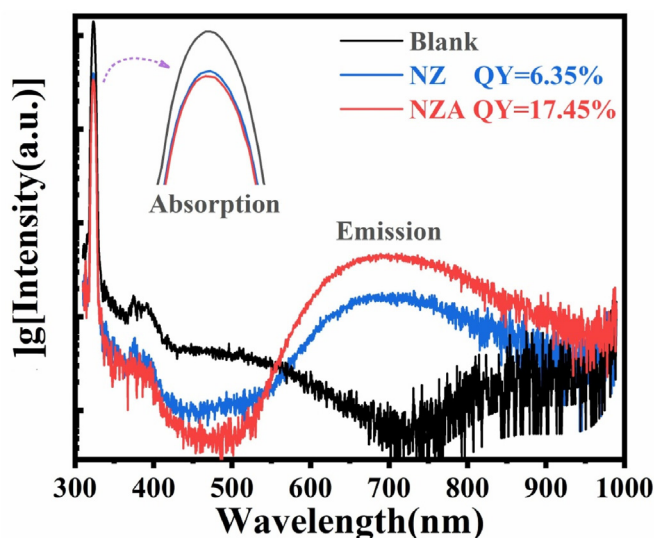


Fig. 4. Quantitative photoluminescence spectra of the QDs glass samples and the reference upon 324 nm excitation to determine the PLQYs.

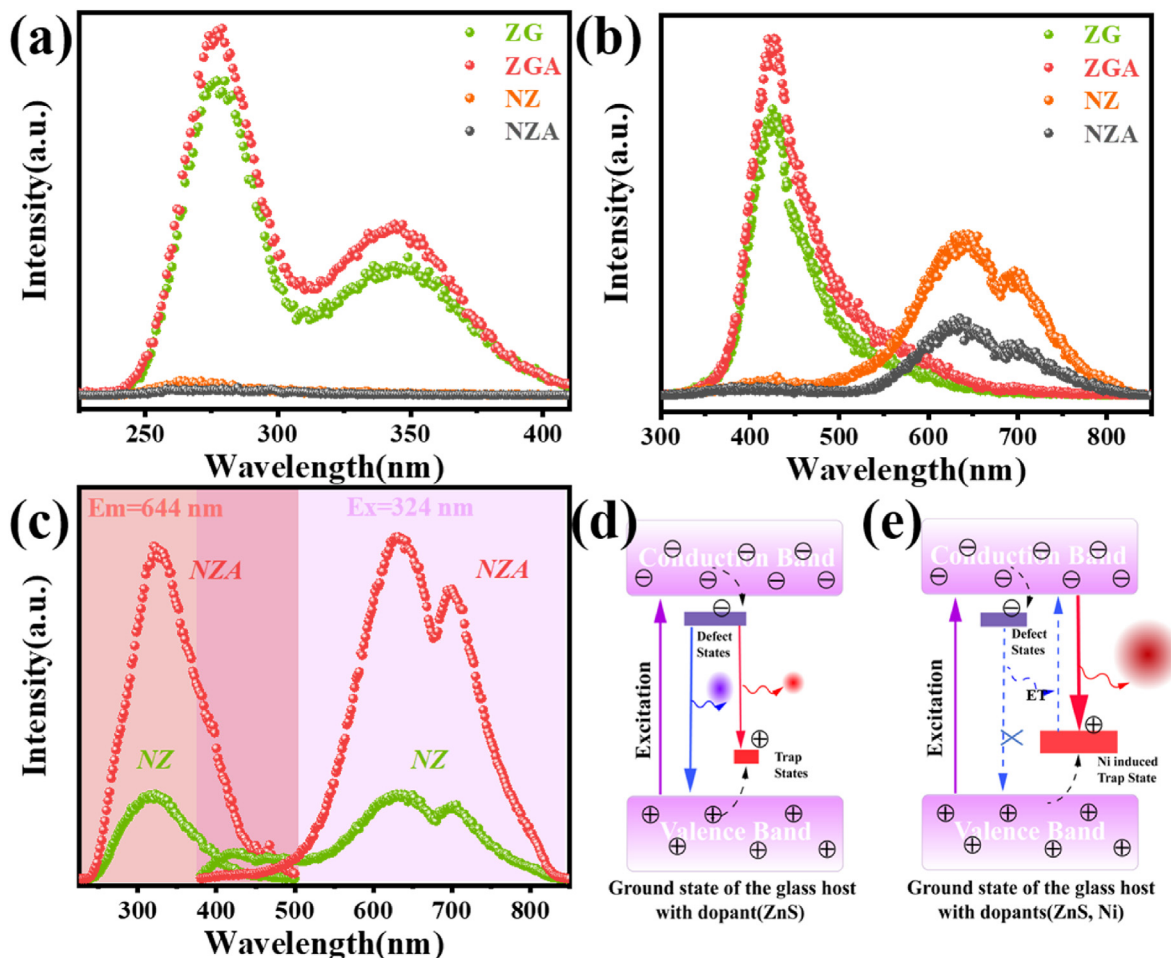


Fig. 5. (a) Excitation spectra of the samples with fluorescence at 427 nm. (b) Photoluminescence spectra of the samples under excitation at 276 nm. (c) Comparison of the excitation spectrum of NZA and photoluminescence spectra under optimal excitation. Schematic of the total energy diagram of the QD glasses in the presence of surface/defect states: excitation and deexcitation processes for undoped structures(d) and those with doped nickel ions(e).

both NZ and NZA have a relatively obvious collapse around 677 nm. In addition, compared to ZG and ZGA, the luminescence intensities of NZ and NZA corresponding to 427 nm were reduced to varying degrees, while the luminescence of NZA in this band almost disappeared.

To better understand the optical properties of the prepared QD glasses, the excitation spectra of all luminescent samples and emission spectra under optimal excitation were recorded. The excitation spectra of the samples at the emission peak at 427 nm has two broad excitation bands, and the excitation effect at 250–300 nm is better, and the excitation peak is around 276 nm, as shown in Fig. 5a. The comparison shows that for the samples doped with ZnS, the excitation spectra of the heat-treated ZGA samples are slightly stronger than those of the ZG samples, while those of the samples co-doped with nickel ions are significantly weaker than those of the ZG and ZGA samples ((both NZ and NZA samples). Among all samples, the excitation spectrum of NZA sample was weakest, almost without excitation peak. The emission spectra of these samples under excitation at 276 nm almost did not change in the trend compared to the emission under excitation at 365 nm, except for the emission in the long-wave range, as shown in Fig. 5b. The fluorescence behavior was not consistent with the 365 nm excitation, the reason being that the wavelength of 276 nm is not the best excitation wavelength for long-wave emission. Therefore, the excitation spectra of samples such as ZGA, NZ, and NZA at

detection wavelengths of 644 and 700 nm were also evaluated, as shown in Fig. S7. Both NZ and NZA samples have wide excitation bands (NZ:250–450 nm, NZA:250–500 nm). The best excitation wavelength is approximately 324 nm. In addition, the excitation spectra of the same sample at different emission wavelengths have the same range except for the difference in intensity. The correspondence between the excitation spectrum intensity and emission intensity of the same sample at different emission wavelengths also shows that the broadband emission of the sample does not originate from the recombination of self-trapped excitons [54]. This can also be explained as the emission peaks of the sample at 644 and 700 nm originate from the same emission center instead of two separate emission centers. This emission center mainly originates from the recombination of electrons in the conduction band with holes trapped by Zn vacancies caused by the entry of nickel ions into the ZnS semiconductor. The comparison of the excitation spectrum of NZA and photoluminescence spectra under optimal excitation can explain the luminescence reductions of NZ and NZA to different degrees at 427 nm. As shown in Fig. 5c, the shortwave emission of the sample coincides with the excitation spectrum of the longwave emission. Therefore, it is worth believing that the released energy belonging to the short-wave emission can be transferred to the electrons on the defect level to make the transition to the conduction band, thereby enhancing the main emission located in the long-wave region, as shown in the simple

schematic of the optical recombination mechanism as Fig. 5e. The PLQYs were determined by the quantitative photoluminescence spectra of the NZ and NZA samples upon 324 nm excitation, and it was found that the PLQY of the NZA sample after heat treatment was significantly improved compared with that of the NZ sample, up to 17.45%, as shown in Fig. 4. This is only a preliminary verification value, and there is still a lot of room for improvement in PLQY through appropriate improvement of the process and preparation conditions. The overlap between the main emission and the main absorption are very small in the excitation-emission spectra curves of NZ and NZA samples, which implies that a very small self-absorption effect existed in this system. The wide absorption and excitation range, large Stokes shift, small self-absorption effect, high PLQY of samples mean that the high-energy short-wave can be high effectively converted into long-wave emission, which can be suitable for energy applications [55]. It is of significance to effectively improve the utilization rate of solar energy when the structure is used as a cover glass for solar cells or processed into a luminescent solar concentrator [56,57].

4. Conclusion

In summary, a new type of environmentally friendly Pb/Cd-free ZnS QD glass based on the inorganic composite amorphous glass has been obtained by the convenient co-melting method. The ZnS QDs in the matrix glass were affected by various nearby functional groups, and were simultaneously protected by the amorphous environment. During the precipitation of ZnS semiconductor in the amorphous glass, trace transition metal nickel ions participated in the induction of defect states, which led to the stable ultra-broad-band deep-red emission of the QD glass. In addition, upon the heat-treatment, more QDs precipitated and grew in the amorphous glass, which implies that more defect states were produced, so that the broad-band emission of the sample was significantly enhanced. This material has broad-band main excitation and emission spectra and minimal self-absorption effect, which can effectively convert the short-wave range into long-wave emission. Thus, the ZnS QD glass material doped with nickel ions can be potentially applied in solid-state lighting, plant growth regulation, color decorative lighting, and other fields, particularly for the improvement in the conversion efficiency of solar cells.

Auther contributions

Zheng Wang: Data curation, Visualization, Writing – original draft. Feifei Huang: Conceptualization, Writing - review & editing. Muzhi Cai: Investigation. Xianghua Zhang: Supervision. Degang Deng: Formal analysis. Shiqing Xu: Funding acquisition, Project administration, Resources.

Declaration of competing interest

The authors declare that they have no known competing financial interests or personal relationships that could have appeared to influence the work reported in this paper.

Acknowledgements

This work was supported by the National Key Research and Development Project of China (2018YFE0207700) and the National Natural Science Foundation of China (NSFC) (61975193, 51872270 and U1909211).

Appendix A. Supplementary data

Supplementary data to this article can be found online at <https://doi.org/10.1016/j.jmat.2022.10.001>.

References

- [1] Selopal GS, Zhao H, Wang ZM, Rosei F. Core/shell quantum dots solar cells. *Adv Funct Mater* 2020;30(13):1908762.
- [2] Zhong H, Wang Y. Quantum dots on demand. *Nat Photonics* 2020;14(2):65–6.
- [3] Gurioli M, Wang Z, Rastelli A, Kuroda T, Sanguinetti S. Droplet epitaxy of semiconductor nanostructures for quantum photonic devices. *Nat Mater* 2019;18(8):799–810.
- [4] Qi H, Wang S, Jiang X, Fang Y, Wang A, Shen H, Du Z. Research progress and challenges of blue light-emitting diodes based on II–VI semiconductor quantum dots. *J Mater Chem C* 2020;8(30):10160–73.
- [5] Kagan CR, Lifshitz E, Sargent EH, Talapin DV. Building devices from colloidal quantum dots. *Science* 2016;353(6302).
- [6] Roh J, Park YS, Lim J, Klimov VI. Optically pumped colloidal-quantum-dot lasing in LED-like devices with an integrated optical cavity. *Nat Commun* 2020;11(1):271.
- [7] Pietryga JM, Park YS, Lim J, Fidler AF, Bae WK, Brovelli S, et al. Spectroscopic and device aspects of nanocrystal quantum dots. *Chem Rev* 2016;116(18):10513–622.
- [8] Li H, Wu K, Lim J, Song H-J, Klimov VI. Doctor-blade deposition of quantum dots onto standard window glass for low-loss large-area luminescent solar concentrators. *Nat Energy* 2016;1(12):16157.
- [9] Sui X, Gao X, Wu X, Li C, Yang X, Du W, Ding Z, Jin S, Wu K, Sum TC, Gao P, Liu J, Wei X, Zhang J, Zhang Q, Tang Z, Liu X. Zone-folded longitudinal acoustic phonons driving self-trapped state emission in colloidal CdSe nanoplatelet superlattices. *Nano Lett* 2021;21(10):4137–44.
- [10] Li M, Xia Z. Recent progress of zero-dimensional luminescent metal halides. *Chem Soc Rev* 2021;50(4):2626–62.
- [11] Shao X, Wang J, Han J, Liu C, Ruan J, Zhao X. Growth kinetics and optical properties of PbSe quantum dots in dual-phase lithium-aluminum-silicate glass ceramic. *J Eur Ceram Soc* 2020;40(12):4122–8.
- [12] Xue J, Wang X, Jeong JH, Yan X. Fabrication, photoluminescence and applications of quantum dots embedded glass ceramics. *Chem Eng J* 2020;383:123082.
- [13] Ma Y, Zhang Y, Yu WW. Near infrared emitting quantum dots: synthesis, luminescence properties and applications. *J Mater Chem C* 2019;7(44):13662–79.
- [14] Becker-Koch D, Albaladejo-Siguan M, Lami V, Paulus F, Xiang H, Chen Z, Vaynzof Y. Ligand dependent oxidation dictates the performance evolution of high efficiency PbS quantum dot solar cells. *Sustain Energy Fuels* 2020;4(1):108–15.
- [15] Chen B, Pradhan N, Zhong H. From large-scale synthesis to lighting device applications of ternary I–III–VI semiconductor nanocrystals: inspiring greener material emitters. *J Phys Chem Lett* 2018;9(2):435–45.
- [16] Bian K, Li R, Fan H. Controlled self-assembly and tuning of large PbS nanoparticle supercrystals. *Chem Mater* 2018;30(19):6788–93.
- [17] Lee H, Leventis HC, Moon S-J, Chen P, Ito S, Haque SA, Torres T, Nüesch F, Geiger T, Zakeeruddin SM, Grätzel M, Nazeeruddin MK. PbS and CdS quantum dot-sensitized solid-state solar cells: “Old concepts, new results.”. *Adv Funct Mater* 2009;19(17):2735–42.
- [18] Xia M, Luo J, Chen C, Liu H, Tang J. Semiconductor quantum dots-embedded inorganic glasses: fabrication, luminescent properties, and potential applications. *Adv Opt Mater* 2019;7(21):1900851.
- [19] Vetchinnikov MP, Lipatiev AS, Shakhgildyan GY, Golubev NV, Ignat'eva ES, Fedotov SS, Lipateva TO, Lotarev SV, Vilkovskiy GA, Sigaev VN. Direct femto-second laser-induced formation of CdS quantum dots inside silicate glass. *Opt Lett* 2018;43(11):2519–22.
- [20] Litvin AP, Babaev AA, Dubavik A, Cherevnikov SA, Parfenov PS, Ushakova EV, Baranov MA, Andreeva OV, Purcell-Milton F, Gun'ko Y, Fedorov AV, Baranov AV. Strong enhancement of PbS quantum dot NIR emission using plasmonic semiconductor nanocrystals in nanoporous silicate matrix. *Adv Opt Mater* 2018;6(6):1701055.
- [21] Huang X, Guo Q, Yang D, Xiao X, Liu X, Xia Z, Fan F, Qiu J, Dong G. Reversible 3D laser printing of perovskite quantum dots inside a transparent medium. *Nat Photonics* 2019;14(2):82–8.
- [22] Liu X, Zhou J, Zhou S, Yue Y, Qiu J. Transparent glass-ceramics functionalized by dispersed crystals. *Prog Mater Sci* 2018;97:38–96.
- [23] Yang B, Mei S, He H, Zhu Y, Hu R, Zou J, Xing G, Guo R. Lead oxide enables lead volatilization pollution inhibition and phase purity modulation in perovskite quantum dots embedded borosilicate glass. *J Eur Ceram Soc* 2022;42(1):258–65.
- [24] Esteve-Turrillas FA, Abad-Fuentes A. Applications of quantum dots as probes in immunosensing of small-sized analytes. *Biosens Bioelectron* 2013;41:12–29.
- [25] Osborne MA, Fisher AA. Charge-tunnelling and self-trapping: common origins for blinking, grey-state emission and photoluminescence enhancement in semiconductor quantum dots. *Nanoscale* 2016;8(17):9272–83.
- [26] Wu P, Yan XP. Doped quantum dots for chemo/biosensing and bioimaging.

- Chem Soc Rev 2013;42(12):5489–521.
- [27] Guria AK, Dutta SK, Adhikari SD, Pradhan N. Doping Mn^{2+} in lead halide perovskite nanocrystals: successes and challenges. *ACS Energy Lett* 2017;2(5):1014–21.
- [28] Jana S, Srivastava BB, Jana S, Bose R, Pradhan N. Multifunctional doped semiconductor nanocrystals. *J Phys Chem Lett* 2012;3(18):2535–40.
- [29] Srivastava BB, Jana S, Pradhan N. Doping Cu in semiconductor nanocrystals: some old and some new physical insights. *J Am Chem Soc* 2011;133(4):1007–15.
- [30] Karan NS, Sarma DD, Kadam RM, Pradhan N. Doping transition metal (Mn or Cu) ions in semiconductor nanocrystals. *J Phys Chem Lett* 2010;1(19):2863–6.
- [31] Silva AS, Lourenco SA, da Silva MA, da Silva SW, Morais PC, Dantas NO. Effect of Co co-doping on the optical properties of ZnTe:Mn nanocrystals. *Phys Chem Chem Phys* 2017;19(2):1158–66.
- [32] Zhang Y, Sun B, Yang L, Lu X, Gao Z, Chu Y, Guo S, Sun S, Zhang S, Li L, Liu L, Yang X, Ren J, Zhang J. Multi-phase induced ultra-broad 1100–2100 nm emission of Ni^{2+} in nano-glass composites containing hybrid ZnGa_2O_4 and ZnF_2 nanocrystals. *J Eur Ceram Soc* 2020;40(5):2229–33.
- [33] Liu M, Wang L, Guan Z, Liu Z, Zhu Y, Tang A. Doping of Cu(i) ions into CdS/ZnS core/shell nanocrystals through a cation exchange strategy. *J Mater Chem C* 2019;7(48):15285–91.
- [34] Bhowal S, Ghosh A, Chowdhuri SP, Mondal R, Das BB. A novel metallogel based approach to synthesize (Mn, Cu) doped ZnS quantum dots and labeling of MCF-7 cancer cells. *Dalton Trans* 2018;47(18):6557–69.
- [35] Duan X, Yuan D, Cheng X, Liu Z, Zhang X. Preparation and optical properties of Co^{2+} -doped $\text{Li}_2\text{O-Ga}_2\text{O}_3\text{-SiO}_2$ glass-ceramics. *J Alloys Compd* 2008;453(1–2):379–81.
- [36] Lorenz S, Erickson CS, Riesner M, Gamelin DR, Fainblat R, Bacher G. Directed exciton magnetic polaron formation in a single colloidal $\text{Mn}^{2+}:\text{CdSe}/\text{CdS}$ quantum dot. *Nano Lett* 2020;20(3):1896–906.
- [37] Chen D, Wan Z, Zhou Y, Ji Z. Cr^{3+} -doped gallium-based transparent bulk glass ceramics for optical temperature sensing. *J Eur Ceram Soc* 2015;35(15):4211–6.
- [38] Chenu S, Véron E, Genevois C, Garcia A, Matzen G, Allix M. Long-lasting luminescent $\text{ZnGa}_2\text{O}_4:\text{Cr}^{3+}$ transparent glass-ceramics. *J Mater Chem C* 2014;2(46):10002–10.
- [39] Wang Z, Huang F, Yang Q, Hua Y, Zhang J, Ye R, Xu S. Efficient controllable NIR-MIR luminescence conversion in optical nanostructured silicate glasses. *J Phys Chem C* 2019;123(23):14662–8.
- [40] Xia M, Liu C, Zhao Z, Ai B, Yin Q, Xie J, Han J, Zhao X. Formation and optical properties of ZnSe and ZnS nanocrystals in glasses. *J Non-Cryst Solids* 2015;429:79–82.
- [41] Chen D, Xu M, Liu S, Li X. $\text{Eu}^{2+}/\text{Eu}^{3+}$ dual-emitting glass ceramic for self-calibrated optical thermometry. *Sensor Actuat B Chem* 2017;246:756–60.
- [42] Dimitrov V, Komatsu T. Classification of simple oxides: a polarizability approach. *J Solid State Chem* 2002;163(1):100–12.
- [43] Wang Z, Huang F, Li D, Lei R, Zhang J, Xu S. An environmental amorphous solid by local crystallization for multifunctional optical applications. *J Clean Prod* 2020;270:122441.
- [44] Mei S, Wei X, Yang D, Su D, Yang W, Zhang G, Hu Z, Yang B, Dai H, Xie F, Zhang W, Guo R. Color-tunable optical properties of cadmium-free transition metal ions doped InP/ZnS quantum dots. *J Lumin* 2019;212:264–70.
- [45] Amani-Ghadim AR, Khodam F, Seyed Dorraji MS. ZnS quantum dot intercalated layered double hydroxide semiconductors for solar water splitting and organic pollutant degradation. *J Mater Chem* 2019;7(18):11408–22.
- [46] Zhou S, Jiang N, Miura K, Tanabe S, Shimizu M, Sakakura M, Shimotsuma Y, Nishi M, Qiu J, Hirao K. Simultaneous tailoring of phase evolution and dopant distribution in the glassy phase for controllable luminescence. *J Am Chem Soc* 2010;132(50):17945–52.
- [47] Li K, Ye Y, Zhang W, Hu Y, Yang Y, Zhou Y, Liu C. Modulation of the optical properties of ZnS QD-embedded glass through aluminum and manganese doping. *J Mater Chem C* 2021;9(34):11261–71.
- [48] Chang L, He X, Chen L, Zhang Y. Mercaptophenylboronic acid-capped Mn-doped ZnS quantum dots for highly selective and sensitive fluorescence detection of glycoproteins. *Sensor Actuat B Chem* 2017;243:72–7.
- [49] Karan NS, Sarkar S, Sarma DD, Kundu P, Ravishanker N, Pradhan N. Thermally controlled cyclic insertion/ejection of dopant ions and reversible zinc blende/wurtzite phase changes in ZnS nanostructures. *J Am Chem Soc* 2011;133(6):1666–9.
- [50] Gao G, Reibstein S, Spiecker E, Peng M, Wondraczek L. Broadband NIR photoluminescence from Ni^{2+} -doped nanocrystalline Ba-Al titanate glass ceramics. *J Mater Chem* 2012;22(6):2582–8.
- [51] Cao J, Guo H, Hu F, Li L, Xu S, Peng M. Instant precipitation of $\text{KMgF}_3:\text{Ni}^{2+}$ nanocrystals with broad emission (1.3–2.2 μm) for potential combustion gas sensors. *J Am Ceram Soc* 2018;101(9):3890–9.
- [52] Lakshminarayana G, Buddhudu S. Spectral analysis of Mn^{2+} , Co^{2+} and $\text{Ni}^{2+}:\text{B}_2\text{O}_3\text{-ZnO-PbO}$ glasses. *Spectrochim Acta* 2006;63(2):295–304.
- [53] Thulasiramudu A, Buddhudu S. Optical characterization of Mn^{2+} , Ni^{2+} and Co^{2+} ions doped zinc lead borate glasses. *J Quant Spectrosc Ra* 2006;102(2):212–27.
- [54] Ma W, Song X, Yin J, Fei H. Intrinsic self-trapped broadband emission from zinc halide-based metal-organic frameworks. *Chem Commun* 2021;57(11):1396–9.
- [55] Debije M. Better luminescent solar panels in prospect. *Nature* 2015;519(7543):298–9.
- [56] Wu K, Li H, Klimov VI. Tandem luminescent solar concentrators based on engineered quantum dots. *Nat Photonics* 2018;12(2):105–10.
- [57] Zhou Y, Benetti D, Fan Z, Zhao H, Ma D, Govorov AO, Vomiero A, Rosei F. Near infrared, highly efficient luminescent solar concentrators. *Adv Energy Mater* 2016;6(11):1501913.



Zheng Wang is currently a Ph.D. candidate in the School of "Matieres, Molecules et Matériaux (3 M)" at University of Rennes, Rennes and the College of Optical and Electronic Technology at China Jiliang University, Hangzhou. His doctoral supervisor are Prof. Xianghua Zhang and Prof. Shiqing Xu. His current research is mainly on the preparation and characterization of optical functional glass and glass-ceramic materials.



Dr. Feifei Huang is currently an associate professor in the College of Optical and Electronic Technology at China Jiliang University, Hangzhou. She received her Ph.D. in Shanghai Institute of Optics and Fine Mechanics, the Chinese Academy of Sciences in 2015. Her current research is mainly on the laser glass fiber, optical temperature sensor, rare earth luminescent material and lithium anode material design.



Prof. Shiqing Xu is currently a professor in the College of Optical and Electronic Technology at China Jiliang University, Hangzhou. He received his Ph.D. in Shanghai Institute of Optics and Fine Mechanics, the Chinese Academy of Sciences in 2005. His current research is mainly on the fiber laser materials and devices, photoelectric sensing materials and devices and LED lighting materials and devices.